International Journal of Mechanical Sciences 228 (2022) 107425

Contents lists available at ScienceDirect

International Journal of Mechanical Sciences

journal homepage: www.elsevier.com/locate/ijmecsci

Suppressing stick–slip oscillations in drill-strings by Modified Integral Resonant Control

James D.J. MacLean, Vahid Vaziri *, Sumeet S. Aphale, Marian Wiercigroch

Centre for Applied Dynamics Research, School of Engineering, University of Aberdeen, Aberdeen, UK

ARTICLE INFO

Keywords:
Nonlinear oscillations
Drill-string dynamics
Robustness
Stability analysis
Damping and tracking control
Modified Integral Resonant Control

ABSTRACT

This paper presents development of a novel control scheme for suppressing stick–slip oscillations of drill-strings. This scheme utilises a Modified Integral Resonant Control (MIRC) with tracking in order to meet a desired drilling velocity. A low-dimensional two degrees-of-freedom drill-string model incorporating bit-rock interactions adopted for an open-loop control, clearly demonstrate presence of unwanted stick–slip responses. Next a detailed design of the MIRC-based damping scheme (without tracking) capable of eliminating this undesired behaviour is presented. Then in order to enhance efficacy, the MIRC-based scheme is combined with an integral tracking controller to show that this combined damping and integral tracking control scheme is not only capable of eliminating stick–slip oscillations but also maintaining the desired drill-bit angular velocity. To highlight the benefits of the proposed combined scheme, it is compared with the recently proposed Sliding-Mode Controller (SMC). Its inherent simplicity, robustness to parameter uncertainty and excellent performance of the proposed combined scheme propels it to be a leading candidate for stick–slip mitigation in drill-strings. To further showcase the efficacy of the proposed control scheme, its closed-loop performance when implemented on an 8-DOF system, has also been discussed.

1. Introduction

Over the years there has been a significant interest in understanding dynamics of drill-strings due to their pivotal role in mineral exploration. These include real-time data gathering via MWD [1] and the development of various FE based models [2–6]. Due to the complex dynamics inherent within drill-strings and their frictional interactions with the borehole, they are highly susceptible to unwanted oscillatory effects and come in three primary forms of torsional [7–10], lateral [9–12] and axial [9,10,13–15] vibration. These problems occur in all types of well configurations (vertical [16,17], directional [17,18] and horizontal [17,19]) and their accompanying drilling methods [20].

These unwanted oscillations present challenges with the drilling procedure and can and will continue to produce downtime on rigs due to the damage they cause entire drill assemblies [21,22]. This paper focuses on a class of torsional vibration known as stick–slip oscillations. Stick–slip is one of the most commonly encountered vibration phenomenon in any type of well and is the most common reason for down-hole tool and tool joint failure [16,23–25]. Stick–slip research has began with the majority of its studies focusing on isolating the stick–slip phenomenon and simplifying to low degrees-of-freedom (DOF) drill-string models [26,27], mainly based on torsional pendulums. The friction model developed for lumped-mass modelling, is a discontinuous switch case by Navarro-López [28,29]. This friction model elegantly captures the stick–slip dynamics while preserving essential bifurcation behaviour caused by changes in an axial force and driving torque. Actual realistic cutting action in drill-strings involve complex delay behaviours that markedly increase system complexity [30]. In this work, the bit-rock interaction model used in this work, as seen in [28,29], does not utilise these delay complexities and rather focuses just on the stick–slip itself in the form of a low DOF model with this switch case bit-rock interaction.

A drill-string can be modelled by a series of rotational spring–mass–dampers connecting the top drive to the drill-bit and such an approach leads to lumped-mass models [26,27], which isolate specific dynamics and allow for controllers to be designed for these problems. In recent years, 2-DOF models are still used for producing and benchmarking novel control methods for stick–slip [31,32] as well being used for researching dynamics involving complex blade patterns on rock cutting [33]. In this paper, a 2-DOF vertical drill-string model is adopted and derived from first principles as the system of choice. The choice to use a 2-DOF model allows for a sufficiently complex system that can exhibit rich dynamics to benchmark novel control schemes. It

* Corresponding author.
E-mail addresses: r02jm18@abdn.ac.uk (J.D.J. MacLean), vahid.vaziri@abdn.ac.uk (V. Vaziri), s.aphale@abdn.ac.uk (S.S. Aphale), m.wiercigroch@abdn.ac.uk (M. Wiercigroch).

https://doi.org/10.1016/j.ijmecsci.2022.107425
Received 29 November 2021; Received in revised form 18 May 2022; Accepted 30 May 2022
Available online 14 June 2022

should be noted that the model chosen is derived from the in-house experimental setup at the University of Aberdeen belonging to the authors of this paper. This experiment on which the model is derived is focused on reproducing torsional dynamics, namely stick–slip in this instance, and as such this work is focused on the stick–slip behaviours pertaining to the experimental model and its accompanying model.

A number of strategies aimed at mitigating stick–slip oscillations have been developed by academia and industry and reported in literature. For example the company Tomax, patented their unique Anti-Stall Tool (AST) described in [34–36], which tackles the stick–slip problem from that of a mechanical design perspective. Should the drill-string undergo any stick while drilling, the Tomax AST by reducing its length decreases the effective Weight On Bit (WOB). A control input whether it is a driving torque, WOB or angular velocity can act as other control parameter to prevent stick–slip. In recent times, the μ-synthesis control method [37–39] has been proposed as a way to overcome stick–slip oscillations, however it is based on linearisation methods, which delivers the expected performance in a very narrow range around the equilibria of interest. Using only the WOB as a control parameter [40] requires knowing the exact WOB being applied at any given instant, which is technically challenging and consequently, this method lacks robustness in face of uncertain values of WOB. Other potential controllers include axial and torsional feedback [41], time-delayed feedback control [42], linear quadratic regulator [43], Kalman filter based full-state feedback [44], adaptive [45] and pole placement technique based on the numerical optimisation method [46]. However, more significant developments are based on PID and PD control techniques and have been widely reported, e.g. by [47–52]. However, all these methodologies can help to increase the operating ranges but they cannot eliminate the stick–slip problem completely. More importantly, none of these control methods is particularly robust to system parameters or bit-rock changes. In order to mitigate the problem of system parameter changes while ensuring steady drilling, Sliding-mode Control (SMC) has been investigated and applied [28,53,54]. Due to its robustness to parameter uncertainties, the SMC has emerged as a benchmark against which all other stick–slip mitigating control schemes are compared. That being said, SMC has one sizeable downside, its inherent complexity in its design procedure. When it comes to porting a control solution to a real life drill-rig, simplicity in tuning and design is of the utmost importance and thus, the SMC has not garnered yet a significant practical application or an industrial interest.

In this paper, a novel approach to tackle the stick–slip is considered by utilising the 'Modified Integral Resonant Control' (MIRC) [55]. The MIRC is a modified version of the IRC damping scheme first developed to mitigate linear system resonances [56], and is capable of imparting a significant damping to nonlinear resonances as well [57]. The MIRC is a simple, first-order controller that works by adding an extra state equation to the system in question and requires no complicated design as required by the SMC. Incidently, the MIRC only requires a selection of the control gain, which is easily achievable via a simple numerical search. Moreover, as the MIRC is of a similar complexity to PID control, this allows for easy implementation. It should also be noted that this controller does not rely on the linearisation of the drill-string model unlike the μ-synthesis control, thus allowing for a more realistic global performance. The rest of the paper is structured as follows; Section 2 presents the experimental setup with results as well as the open-loop model for the drill-string and classifies all the different parameters while demonstrating its well known open-loop behaviour, Section 3 introduces the MIRC structure and demonstrates how it is added to the drill-string model presented in Section 2. Section 4 introduces the addition of tracking control to the MIRC's structure. Then the robust nature of the combined control scheme of MIRC and tracking control are discussed in Section 5. Section 6 is devoted to the direct comparison between the SMC and MIRC-based damping with integral tracking control in order to draw comparisons in performance and also demonstrates the MIRC-based damping with integral tracking control on a much more complex 8-DOF system. Section 7 concludes the paper. However, the stability analysis and system parameters are presented in the Appendices.

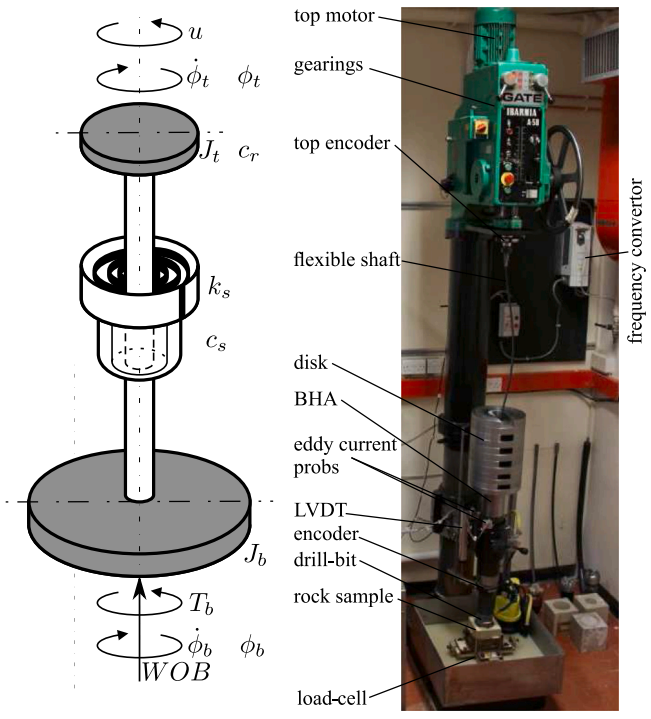

Fig. 1. University of Aberdeen Drill-string Rig and its components. The photograph of the vertical drill-string assembly shows the main parts including actuator (top motor), BHA, drill-bit, rock sample and sensors. The schematic on the left depicts a 2-DOF model of a drill-string represented as a connected series of rotating pendula featuring a highly nonlinear opposing bit-rock interaction torque T_b and weight-on-bit WOB.

2. Experimental results and open-loop analysis

The University of Aberdeen's vertical drill-string rig is shown in Fig. 1 along with the accompanying 2-DOF model [2,54]. This rig can be used in several configurations such as (i) rigid-shaft setup for bit-rock interactions investigation, (ii) flexible shaft setup with no lateral motion for the torsional vibration mode only analysis, (iii) full mode, which mimics all types of drill-string vibration. We have utilised here the first and second configurations for the bit-rock model and stick–slip model calibration in the current work. The main components of the rig are as follows, actuators (top motor), Bottom-Hole-Assembly (BHA), drill-bit and rock sample. The sensors used in this study to record include a four component load-cell, the top and bottom encoders, eddy current probes and a Linear Variable Displacement Transducer (LVDT).

Fig. 2 shows an example of stick–slip oscillations experimentally recorded and occurring for WOB = 1.76 kN and top-torque of 40 N m. Fig. 2(a) and (b) present the time histories of the angular velocities at the bottom, $\dot{\phi}_b$, and the top, $\dot{\phi}_t$, phase portraits from experimental studies. While panels (e) and (f) depict the simulation results from a calibrated low-dimensional model. Their 5 s zoomed-in views are in (c) and (g) together with TOB recorded in the experiment (b) and modelled (d) by Eq. (3) which will described later in the next section. All the model parameter identified from the experimental setup are in the Table 1.

If one is to fully understand the importance of the problems inherent with stick–slip, it is imperative to examine and explore the rich dynamics of the leading to the stick–slip issue. The behaviour of stick–slip and other notable dynamics of constant drilling and stick are explored in this section in detail. The set of differential equations which describe the model are:

$$J_t\ddot{\phi}_t + \left(c_s + c_r\right)\dot{\phi}_t + k_s\phi_t - c_s\dot{\phi}_b - k_s\phi_b = u, \tag{1}$$

$$J_b\ddot{\phi}_b + c_s\dot{\phi}_b + k_s\phi_b - c_s\dot{\phi}_t - k_s\phi_t = -T_b. \tag{2}$$

Table 1
Parameters used for numerical simulation of low dimensional model.

Symbol	Name	Value(s) and Units
μ_{cb}	Coulomb friction coefficient	0.0597
μ_{sb}	Static friction coefficient	0.0843
R_b	Bit radius	0.0492 m
WOB	Weight-on-bit	1760 N
γ_b	Velocity decrease rate	0.3
v_f	Velocity constant	0.1935
ζ	Small positive constant	10^{-6}
u	Top-torque	$u \in [0, 60]$ N m
J_t	Top-drive inertia	13.93 kg m^2
J_b	Bit inertia	1.1378 kg m^2
c_r	Top-drive damping coefficient	11.38 N m s rad^{-1}
c_s	Torsional damping coefficient	0.005 N m s rad^{-1}
k_s	Torsional stiffness coefficient	10 N m rad^{-1}

Table 2
Model parameters and their definitions.

Symbol	Name	Expression/Range of values
τ_r	Reaction torque	$\tau_r := c_b\left(\dot{\phi}_t - \dot{\phi}_b\right) + k_b\left(\phi_t - \phi_b\right)$
τ_s	Static friction torque	$\tau_s := \mu_{sb} R_b WOB$
μ_b	Dry friction coefficient	$\mu_b := \mu_{cb} + \left(\mu_{sb} - \mu_{cb}\right) e^{-\gamma_b \lVert\dot{\phi}_b\rVert / v_f}$
sgn(x)	Signum function	$\operatorname{sgn}(x) = \begin{cases} -1 & \text{if } x < 0 \\ 0 & \text{if } x = 0 \\ 1 & \text{if } x > 0 \end{cases}$
$\lVert x\rVert$	Absolute value function	$\lVert x\rVert = \begin{cases} -x & \text{if } x < 0 \\ x & \text{if } x \geq 0 \end{cases}$

The friction model for T_b used is defined as follows [26]:

$$T_b = \begin{cases} \tau_r, & \text{if } \lVert\dot{\phi}_b\rVert < \zeta \text{ and } \lVert\tau_r\rVert \leq \tau_s \\ \tau_s \operatorname{sgn}\left(\tau_r\right), & \text{if } \lVert\dot{\phi}_b\rVert < \zeta \text{ and } \lVert\tau_r\rVert > \tau_s \\ \mu_b R_b WOB \operatorname{sgn}\left(\dot{\phi}_b\right), & \text{if } \lVert\dot{\phi}_b\rVert \geq \zeta. \end{cases} \tag{3}$$

The adopted friction model operates the drill-string in one of the three distinct phases. Phase 1 is the stick in which the bit is not rotating ($\dot{\phi}_b < \zeta$) as the static friction torque τ_s exceeds or is equal to the reaction torque τ_r: $\lVert\tau_r\rVert \leq \tau_s$. Phase 2 is the transition from the stick to the slip in which the bit just about to rotate again ($\dot{\phi}_b < \zeta$) as the static friction torque τ_s is less than the reaction torque τ_r: $\lVert\tau_r\rVert > \tau_s$. Phase 3 is the slip in which the bit begins to move ($\dot{\phi}_b \geq \zeta$) and cuts into the rock. Table 2 presents the relevant mathematical expressions/ranges for all the system parameters: For simulation purposes, Eqs (1), (2) and the friction model (3), can be seen as generating three separate state-space models in which the system can discontinuously switch between, based on initial conditions, WOB and u. In order to numerically simulate Eqs (1) and (2), the following state-variables are defined:

$$X = \begin{bmatrix} \dot{\phi}_t, & \phi_t - \phi_b, & \dot{\phi}_b \end{bmatrix}^T = \begin{bmatrix} x_1, & x_2, & x_3 \end{bmatrix}^T. \tag{4}$$

Eqs (1) and (2) can be re-described as a state-space system which separates the linear portions and the nonlinear bit-rock interactions model T_b in terms of appropriate matrices as follows:

$$\dot{X} = \begin{bmatrix} \left(c_s + c_r\right)/J_t & -k_s/J_t & c_s/J_t \\ 1 & 0 & -1 \\ c_s/J_b & k_s/J_b & -c_s/J_b \end{bmatrix} X + \frac{u}{J_t}\begin{bmatrix} 1 \\ 0 \\ 0 \end{bmatrix} - \frac{T_b}{J_b}\begin{bmatrix} 0 \\ 0 \\ 1 \end{bmatrix} \tag{5}$$

To infer some important information about the drill-string model, the equilibria of the system should be considered. There exist two distinct equilibria, namely the constant drilling and the stick equilibria respectively. Consider the case of stick in which the top-drive and bit-head velocities are zero respectively ($x_1 = x_3 = 0$) and the state variable derivative is also zero ($\dot{X} = 0$ and) in Eq. (4). Then the equilibrium for $x_{2,e}$ is;

$$x_{2,e} = \frac{u}{k_s}. \tag{6}$$

This translates to an overall equilibrium vector $X_{e,s}$ as follows:

$$X_{e,s} = \begin{bmatrix} 0, \frac{u}{k_s}, 0 \end{bmatrix}^T. \tag{7}$$

Now consider the case of constant drilling in which the top-drive and bit-head velocities are some positive constant Ω_c respectively ($x_1 = x_3 = \Omega_c$) and the state variable derivative is also zero ($\dot{X} = 0$ and $x_1 = x_3 = \Omega_c$) in Eq. (4). Then the equilibrium $x_{2,e}$ can be shown to be:

$$x_{2,e} = \frac{u - c_r\Omega_c}{k_s}. \tag{8}$$

This translates to an overall equilibrium vector $X_{e,c}$ as follows:

$$X_{e,c} = \begin{bmatrix} \Omega_c, \frac{u - c_r}{k_s}, \Omega_c \end{bmatrix}^T. \tag{9}$$

With these system equilibria demonstrated, the behaviour of Eq. (4) and the aforementioned bit-rock model (3) is shown in Fig. 3. As can be seen in Fig. 3(d), stick–slip and constant drilling attractors co-exist within the region bound of $u \in [9, 56]$ N m while $u \in [57, 60]$ N m denotes region where the drill-string only operates in the constant drilling mode. Another important point to note is that as shown in the basins of attraction plotted in Fig. 3(e), the parameter-space defined by the range of initial conditions analysed herewith is dominated by stick–slip attractors. With the adopted drill-string and bit-rock models validated via the simulation results shown in Fig. 3, this work proceeds to design and implementation of the Modified Integral Resonant Control (MIRC) damping scheme aimed at eliminating the unwanted stick–slip oscillations.

3. Modified integral resonant control

To mitigate and suppress stick–slip on the aforementioned system seen in Fig. 1, a Modified Integral Resonant Control scheme is introduced. The scheme is added to the drill-string model and its impact on the equilibria of the new closed-loop system is discussed in detail. Lyapunov stability is also derived and discussed along with simulations to verify its stick–slip suppressing characteristics. A new controller state ψ is defined and then embedded into Eqs (1) and (2) by generating an extra state differential equation. A full derivation for combining the scheme with the drill-string can be found in the Appendix. Consequently, the new scheme modified system dynamics work by adding the control input of MIRC to the original top-torque input u, while additionally adding an extra state equation to the overall system dynamics. The new equations can be described by:

$$J_t\ddot{\phi}_t + \left(c_s + c_r\right)\dot{\phi}_t + k_s\phi_t - c_s\dot{\phi}_b - k_s\phi_b = u + \eta\psi, \tag{10}$$

$$J_b\ddot{\phi}_b + c_s\dot{\phi}_b + k_s\phi_b - c_s\dot{\phi}_t - k_s\phi_t = -T_b, \tag{11}$$

$$\dot{\psi} + \eta\kappa\psi + \lambda\left[\dot{\phi}_b - \dot{\phi}_t\right] = 0. \tag{12}$$

To aid in simulation, a state-vector $\bar{X}$ includes the controller variable:

$$\bar{X} = \begin{bmatrix} \dot{\phi}_t, & \phi_t - \phi_1, & \dot{\phi}_1, & \psi \end{bmatrix}^T = \begin{bmatrix} x_1, & x_2, & x_3, & x_4 \end{bmatrix}^T. \tag{13}$$

This redefinition allows the aforementioned Eqs (10), (11) and (12) to be re-written as a closed-loop state-space system as follows:

$$\dot{\bar{X}} = \begin{bmatrix} \left(c_s + c_r\right)/J_t & -k_s/J_t & c_s/J_t & \eta/J_t \\ 1 & 0 & -1 & 0 \\ c_s/J_b & k_s/J_b & -c_s/J_b & 0 \\ \lambda & 0 & -\lambda & -\kappa\eta \end{bmatrix} \bar{X} + \frac{u}{J_t}\begin{bmatrix} 1 \\ 0 \\ 0 \\ 0 \end{bmatrix} - \frac{T_b}{J_b}\begin{bmatrix} 0 \\ 0 \\ 1 \\ 0 \end{bmatrix} \tag{14}$$

By incorporating the scheme in question, there exists a new state which will possess its own behaviour when the system reaches a new equilibrium in addition to the previously derived equilibria. To analyse the behaviour of the modified drill-string, the equilibria of the controlled system needs to be explored. To this end, consider the case in which the top-drive and bit-head velocities are zero ($x_1 = x_3 = 0$) and the

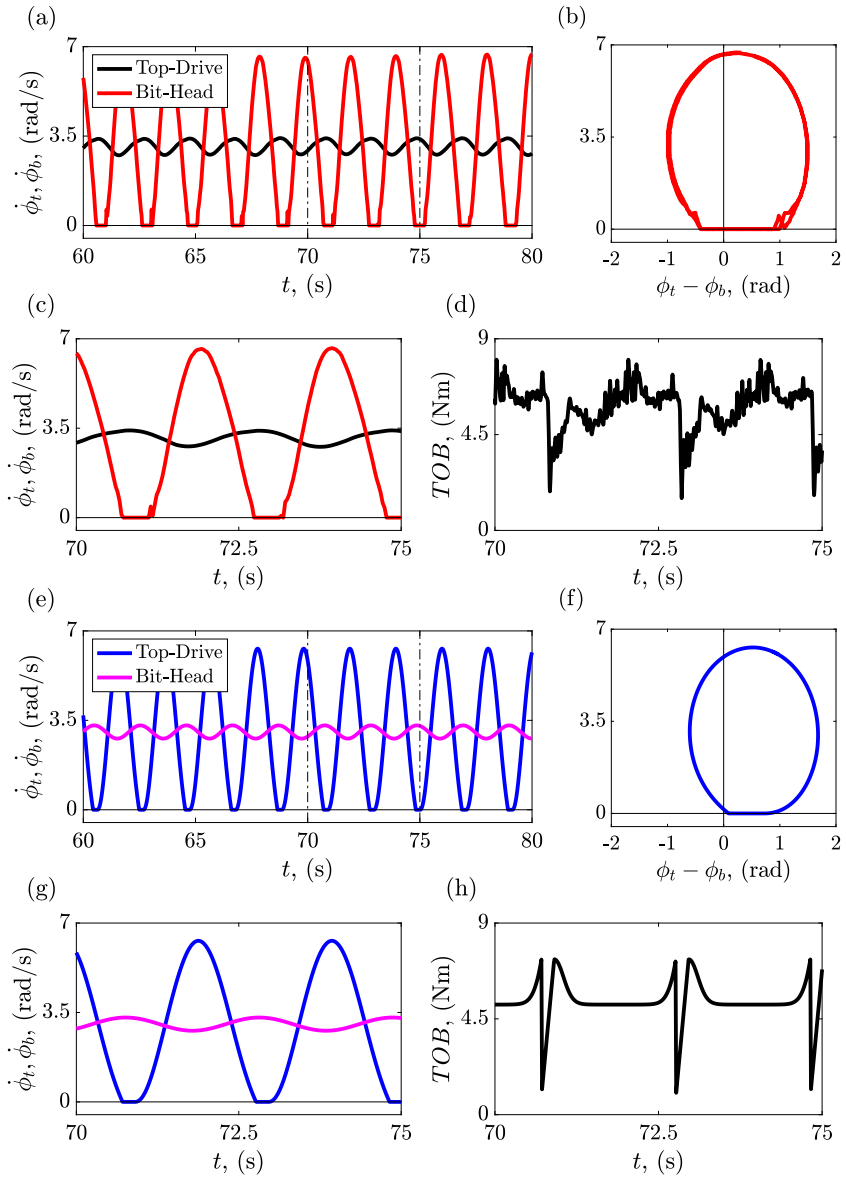

Fig. 2. An example of stick–slip oscillations occurring for WOB = 1.76 kN and top-torque of 40 N m. The time histories of the angular velocities at the bottom, $\dot{\phi}_b$, and the top, $\dot{\phi}_t$, phase portraits and TOB obtained from experimental studies are shown in panels (a), (b), (c) and (d). Their modelled equivalents simulated for a low dimensional model are depicted in panels (e) to (h).

state variable derivative $\dot{\tilde{X}} = 0$ in Eq (14). Looking specifically at the incorporated differential equation:

$$\dot{x}_4 = -\kappa\eta x_4 - \lambda\left[x_3 - x_1\right]. \tag{15}$$

Given that $\dot{\tilde{X}} = 0$, it can be shown that the modified equilibria $x_{4,e}$ is:

$$x_{4,e} = \frac{\lambda}{\kappa\eta}\left[x_1 - x_3\right]. \tag{16}$$

Then the modified equilibria $\bar{X}_{e,s}$ for stick, by substituting in $x_1 = x_3 = 0$ into Eq. (16), is:

$$\bar{X}_{e,s} = \left[0, \frac{u}{k_s}, 0, 0\right]^T. \tag{17}$$

The modified equilibria $\bar{X}_{e,c}$ for constant drilling can be found similarly by substituting $x_1 = x_3 = \Omega_c$ into Eq. (16):

$$\bar{X}_{e,c} = \left[\Omega_c, \frac{u}{k_s}, \Omega_c, 0\right]^T. \tag{18}$$

Since the scheme works by adding an extra state to the open-loop dynamics of the drill-string, it follows that the same system attractors exist and are not altered in their unique behaviours. This is evidenced by the equilibria of x_1, x_2 and x_3 not changing even under the influence of the scheme. When the system reaches either of the constant drilling or stick attractors, the control input $u + \eta x_4 \to u$, once it has settled. In the Appendix, there a Lyapunov stability analysis is carried out should the reader wish to view it. The figure overleaf demonstrates the effects that scheme on the natural system response of stick–slip. The following table details the gains used for the simulations seen overleaf.

Table 3
MIRC gain values.

Symbol	Name	Value
λ	Output feedback gain	−22
η	Integrator gain	10
κ	Feed-through gain	1

Fig. 4(a) shows the stick–slip limit cycle in open-loop for $u = 40$ N m. The scheme is turned on at $t = 75$ s and as shown, the system is driven to its corresponding (inherent) constant drilling attractor at

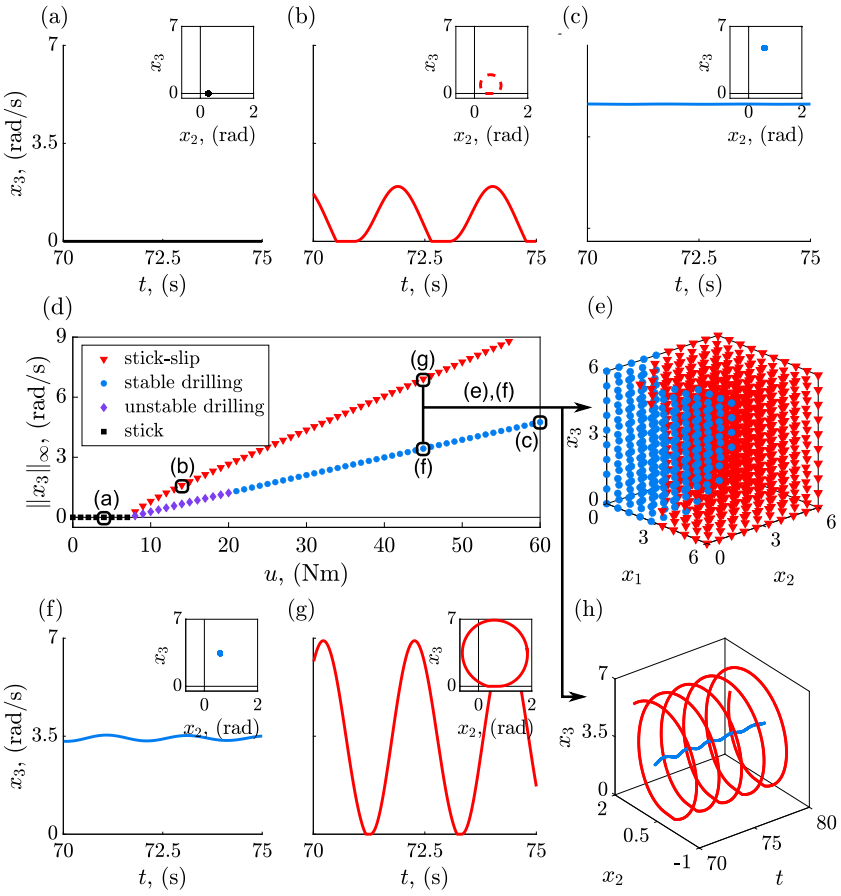

Fig. 3. Bit velocity vs. time traces for (a) stick ($u = 3$ N m), (b) stick–slip ($u = 15$ N m) and (c) constant drilling ($u = 60$ N m). (d) The complete open-loop bifurcation diagram showing the three attractors as stick ($u \in [0, 7]$ N m → black squares), stick–slip ($u \in [9, 57]$ N m → red triangles), unstable constant drilling ($u \in [9, 20]$ N m → purple diamonds) and stable constant drilling ($u \in [21, 60]$ N m → blue circles). (e) 3D Basins of Attraction plot indicates state values where stable drilling and stick–slip occur. (f) and (g) Time histories and portraits where the co-existing constant drilling with stick–slip attractors computed for $u = 45$ N m exist. (h) A 3-D phase-plane portrait of the same dynamics is shown. The region of $u \in [9, 20]$ N m possesses an unstable constant drilling branch not accessible practically (or via traditional numerical integration) except with the method of numerical continuation or closed-loop control.

$\Omega_c = 2.993$ rad s^{-1}. Fig. 4(b) plots the 2-D phase-plane portrait that corresponds to the dynamics presented in Fig. 4(a) and explains how the controlled system is being driven to constant drilling. Fig. 4(c) shows the corresponding 3D perspective with respect to time, for more clarity. Fig. 4(e) plots the control input required before and after the activation. When the scheme is turned on at $t = 75$ s the control input undergoes a brief period of transients and soon settles to the same open-loop torque value. This demonstrates that the scheme acts by supplementing the drill-string system with its own dynamics without changing the inherent constant response. Fig. 4(f) details the control block diagram of the implemented scheme (damping only) whilst Fig. 4(g) shows how all the basins of attraction within the same range of initial conditions as that analysed for in Fig. 3(e) change to constant drilling under the influence of the implemented scheme. This clearly demonstrates the effectiveness of the scheme in suppressing unwanted stick–slip oscillations.

A key result that requires an in-depth probing is the ability of this scheme to stabilise and reach any the unstable constant drilling solution. Unstable constant drilling branches have been shown to exist in drill-string structures and are usually presented as solutions only accessible via numerical continuation methods. By using the scheme in question, these instances of unstable constant drilling attractors, occurring in open-loop, are successfully stabilised by the scheme and made reachable. To further clarify the dynamics in this region, see Fig. 5. When the scheme is engaged, the stick–slip attractor is suppressed and a new constant-drilling attractor becomes reachable by the controlled drill-string. There are small oscillations of the control input seen in the zoomed insert in Fig. 5(b) that confirms the stabilisation of this solution. When the scheme is turned off, this newly stabilised solution loses its stability as the system effectively becomes that of an open-loop drill-string once more. This is also verified by the control input settling back to $u = 15$ N m. In conclusion, to stabilise this region where unstable constant drilling attractors exist in open-loop, the scheme is required to be engaged at all times. In this particular system type, the existence of a Hopf bifurcation is shown by Navarro-López [30] which is critical to following heuristic argument presented with respect to the MIRC detailed. To understand why this stabilisation occurs, a discussion into super-critical Hopf bifurcations is required. Consider the following normal form for the Hopf bifurcation when in closed-loop with the scheme:

$$\dot{r} = \mu r - \|r\|^2 r + \eta\psi + \text{h.o.t}, \tag{19}$$

$$\dot{\psi} = \lambda r - \kappa\eta\psi, \tag{20}$$

where $\mu > 0$. If the higher-order-terms (h.o.t) are ignored and Eqs (19) and (20) are examined at equilibrium, consider the following equilibria variables of r_e and ψ_e respectively;

$$0 = \mu r_e - \|r_e\|^2 r_e + \eta\psi_e, \tag{21}$$

$$0 = \lambda r_e - \kappa\eta\psi_e. \tag{22}$$

This allows for the new equilibria of (19) to be solved for as follows by rearranging (22) for ψ_e and substituting it into (21). For simplicity by assuming that $r_e > 0$, the absolute value square term can be simply

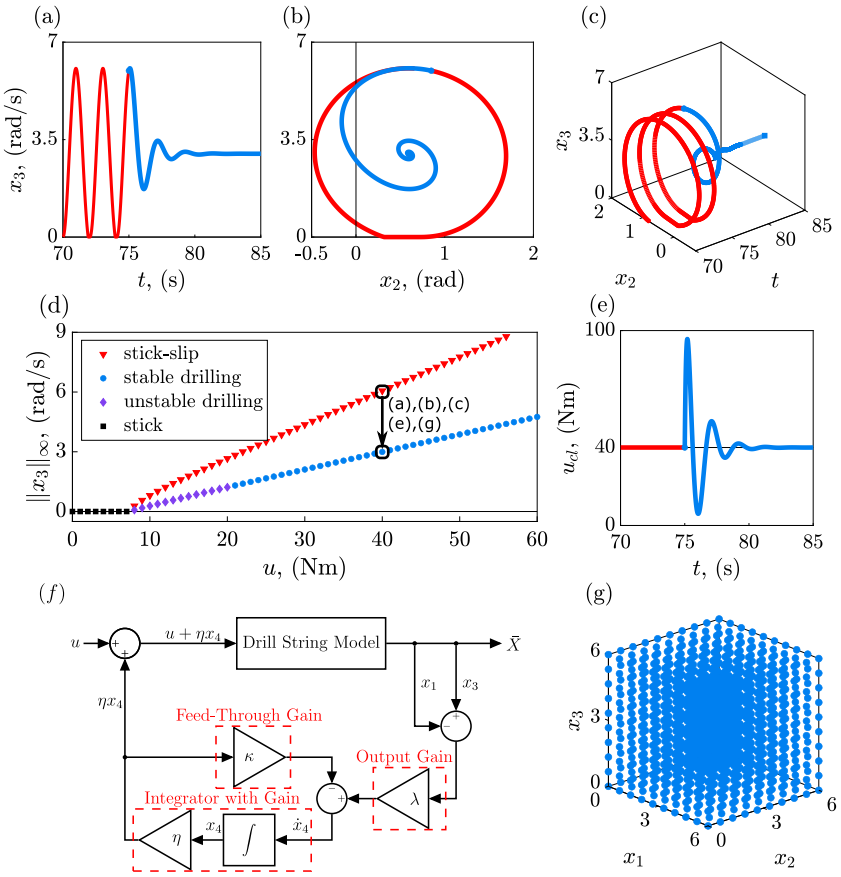

Fig. 4. An overview of the MIRC method and its effect on the system dynamics. The open loop responses is in red and the closed-loop one is in blue. (a – c) Shows the time–history, 2-D and 3D phase-portraits for $u = 40$ N m, respectively. (d) The complete bifurcation diagram showing all three types of behaviour. (e) An example of the control input versus time. Please note the initial and final control input (top) is 40 N m. (f) The scheme's block diagram construction. (g) 3D Basins of attraction of closed-loop system.

thought of as r_e^2 resulting in:

$$\psi_e = \frac{\lambda}{\kappa\eta} r_e, \tag{23}$$

$$0 = \left(\mu + \frac{\lambda}{\kappa}\right) r_e - r_e^3. \tag{24}$$

Solving for the equilibria r_e,

$$r_e \left(\mu + \frac{\lambda}{\kappa} - r_e^2\right) = 0 \rightarrow r_{e1} = 0,\ r_{e2,3} = \pm\sqrt{\mu + \frac{\lambda}{\kappa}}. \tag{25}$$

By analysing (25), if $\mu > 0$ and $\lambda = \kappa = 0$ simultaneously, there exist the two stable equilibria exist at $r_{e2,3} = \pm\sqrt{\mu}$ which corresponds to a stable limit cycle. Around this stable limit cycle, there is the unstable equilibrium of $r_{e1} = 0$ which the limit cycle oscillates around. If in the closed-loop case λ and κ are chosen such that $\mu + \lambda/\kappa > 0$, then this serves to keep the equilibria stability the same, but has the effect of increasing the amplitude of the limit cycle. If on the other hand, λ and κ are chosen such that $\mu + \lambda/\kappa < 0$, then this collapses $r_{e2,3}$ to be complex solutions which results in the remaining real equilibria $r_{e1} = 0$ to become a stable solution. If knowledge of μ exists, then it is easy to choose λ and κ that allow for this second condition to exist and thereby re-stabilise the $r_{e1} = 0$ equilibrium. The following simulations show the bifurcation diagrams for Eqs (19) and (20) as well as a time–history example showing the effects of the scheme:

In the open-loop case, for $\mu \leq 0$, all equilibria are stable and for $\mu > 0$ unstable solutions arise with pairs of stable solutions representing the Hopf limit cycle. Fig. 6(c) shows the evolution of the Hopf normal form to the positive solution r_e^2 and then highlights the stabilisation effects of the scheme when activated at $t_{on} = 2$ s. In conclusion, the scheme is capable of directly affecting the stability of equilibria for Hopf bifurcations. In the following subsection, the basic linear frequency characteristics of the open-loop and closed-loop system is discussed. Though the stick–slip damping capabilities of the scheme are noteworthy, where it really excels is its ability to accommodate an additional tracking loop, thereby ensuring that a desired (reference) drill-bit velocity can be met and maintained at all times. Consequently, the scheme's damping capabilities will be combined with an integral tracking in the following section.

4. Implementation of integral tracking with the MIRC

Normal operations require that certain desired bit and top-drive velocities are consistently maintained in order to ensure safe and efficient operation [58,59]. In this section, the MIRC scheme, as shown in Fig. 4(f), is combined with an integral tracking loop in order to maintain a desired reference speed Ω_d (See Fig. 7). In order to do this, a new state vector $\hat{X}$ is defined as follows:

$$\hat{X} = \begin{bmatrix}\dot{\phi}_t, & \phi_t - \phi_1, & \dot{\phi}_1, & \psi, & \gamma\end{bmatrix}^T = \begin{bmatrix}x_1, & x_2, & x_3, & x_4 & x_5\end{bmatrix}^T, \tag{26}$$

where the new state γ represent the integral tracking variable. Modifying Eq. (14) with this integral tracker is as simple as adding a new state, expanding the matrices accordingly and by adding a desired reference velocity Ω_d with which to track:

$$\dot{\hat{X}} = \begin{bmatrix} (c_s + c_r)/J_t & -k_s/J_t & c_s/J_t & \eta/J_t & k_i/J_t \\ 1 & 0 & -1 & 0 & 0 \\ c_s/J_b & k_s/J_b & -c_s/J_b & 0 & 0 \\ \lambda & 0 & -\lambda & -\kappa\eta & 0 \\ -1 & 0 & 0 & 0 & 0 \end{bmatrix} \hat{X} + \frac{u}{J_t} \begin{bmatrix} 1 \\ 0 \\ 0 \\ 0 \\ 0 \end{bmatrix}$$

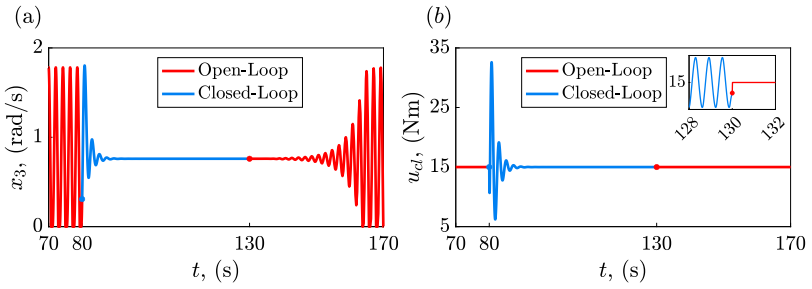

Fig. 5. The effects of turning on (t = 80 s) the MIRC acts to stabilise the unstable solution and then turning off (t = 130 s) the MIRC results in going back to the stick–slip oscillations. (a) shows the bit angular velocity and (b) presents the control input. Please not the initial and final control signal (top torque) is 15 N m in which the system has one stable and one unstable solution (see Fig. 4).

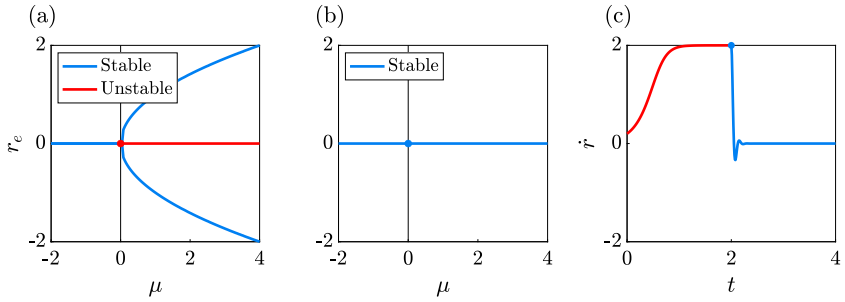

Fig. 6. Nonlinear dynamics stability analysis of the system with MIRC control. (a) and (b) Classical Hopf bifurcation and its disappearance by an introduction of the MIRC in the region of $\mu \in [-1, 4]$. (c) The effect of the MIRC being turned on at $t = 2$ s. Simulation was conducted for $\mu = 4$, $\lambda = -50$, $\kappa = 1$ and $\eta = 25$.

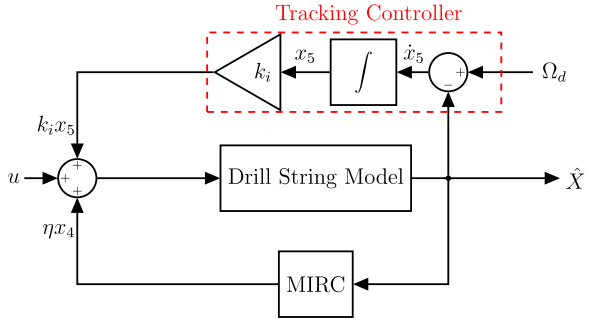

Fig. 7. Structure of the combined MIRC with integral tracking controller. The tracking controller is added to the MIRC presented in Fig. 4(f) where the input parameter of this controller is the drill-bit desired velocity Ω_d.

$$-\frac{T_b}{J_b}\begin{bmatrix}0\\0\\1\\0\\0\end{bmatrix}+\Omega_d\begin{bmatrix}0\\0\\0\\0\\1\end{bmatrix}. \tag{27}$$

The equilibria remain the same as before and the details of the Lyapunov stability analysis for this combined scheme can be seen in the Appendix. An example of a detailed closed-loop dynamic performance of the MIRC-based damping and tracking control scheme is presented in Fig. 8. To test the new combined scheme, the previous gains for the MIRC portion is kept the same as in Table 3, and the integral tracking gain is set as follows, $k_i = 10$.

(a) Time trace of the bit velocity for the open-loop drill-string operating in the stick phase, when commanded to achieve the desired bit velocity of $\Omega_d = 3.5$ rad s^{-1}. (b) Time traces of the bit velocity for the open-loop drill-string operating in the stick phase with an unstable constant drilling attractor. The combined scheme demonstrates the ability to stabilise unstable constant drilling attractors as well as provide damping for stick–slip phenomenon. (c) and (g) Time traces of the bit velocity for the open-loop drill-string operating at a point in the coexisting attractors (stick–slip and constant drilling) region, when commanded to achieve the desired bit velocity of $\Omega_d = [2.993, 2.111]$ rad s^{-1}, respectively. (d) Bifurcation diagram of the closed-loop drill-string. It is clear from the traces plotted in Fig. 8, that the MIRC-based damping and tracking scheme performs excellently in ensuring the total elimination of stick–slip oscillations and additionally, guarantees that the drill-bit achieves the desired bit velocity. As the drill-string (due to its interaction with the bore-wall) and the nature of the rock strata being drilled, the overall drill-bit with bit-rock interaction is a system with significant parameter uncertainty. As such, no control scheme is of any consequence unless it demonstrates significant robustness to parameter uncertainty. The linear IRC scheme has significant inherent robustness [60] and therefore, it is expected that a similar level of robustness is demonstrated by the proposed combined scheme utilised herewith. To explore and validate the control scheme's robustness, a detailed analysis of the closed-loop system's performance to significant parameter variation is carried out. These results are presented in the following section.

5. Robustness analysis

In order to demonstrate the robustness of the combined scheme, it is essential to determine how changing key system parameters affects the closed-loop response while keeping the scheme's gains the same. Changing significant system parameters will cause the system dynamics to change accordingly. As a result, this can change the location of: constant drilling solutions, stick and stick–slip solutions found within the system. If the combined scheme can still maintain constant drilling under changing system parameters, then it possesses robustness within this context of drilling.

The following parameters, namely: the top-drive inertia J_t, top-drive damper c_r, torsional spring stiffness k_s, and torsional damper c_s are varied in their values by set percentages of: ±10%, ±20% and ±30%. Fig. 9 presents simulation results for cases where the parameters were changed by −10%, −20% and −30% (parameter values are individually

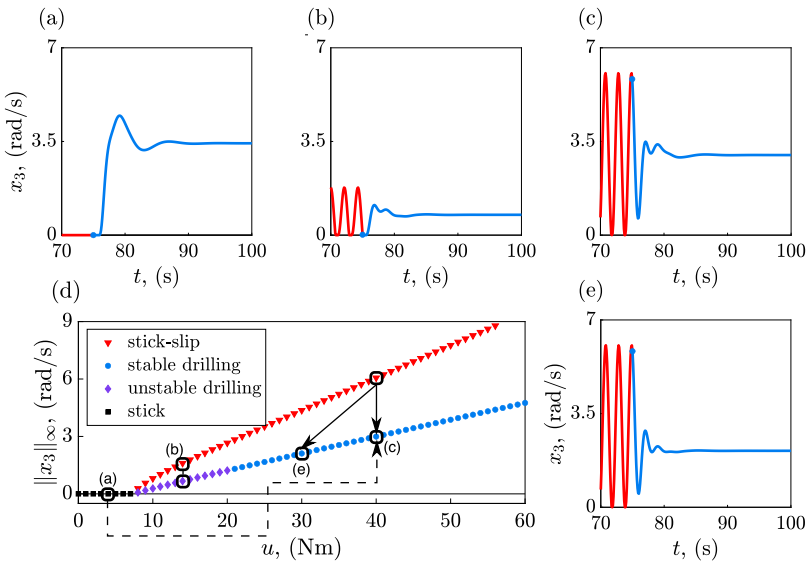

Fig. 8. An overview of the MIRC method with tracking and its effect on the system dynamics. The open loop responses is in red and the closed-loop one is in blue and magenta. (a) and (b) Show the time history for moving from stick to constant drilling for the cases with and without stable constant trajectories, respectively. (c) and (c) Show the time histories of two cases of tracking low and low desired velocities.

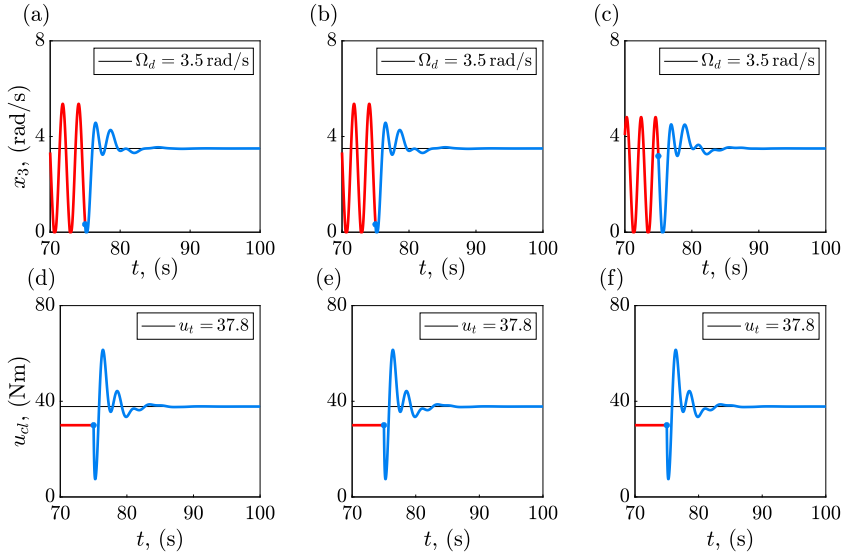

Fig. 9. Black solid lines represent target desired velocities and torques for respective plots. Time traces for bit velocity and corresponding control input for system with: (a and d) 70% of the nominal values. (b and e) 80% of the nominal values. (c and f) 90% of the nominal values.

reduced to 70%, 80% and 90% of the nominal values as listed in Table 1).

The combined scheme is able to guide the system to the desired bit velocity Ω_d in each case. It must be noted that for each of the cases, the control input required to ensure that the desired bit velocity is achieved varies. As a result, though in all three cases, the desired bit velocity is set to $\Omega_d = 3.5\ \mathrm{rad\,s^{-1}}$, the control torque needed to achieve this desired bit velocity is 33.82 N m, 37.80 N m and 41.78 N m for changed parameter values of 70%, 80% and 90% of the nominal value set. Note that as system parameters decrease from their nominal values, the location and consequently, the natural velocities of constant drilling attractors found within the system will also change. A similar set of simulations were run to look at how the closed-loop system performs when the system parameters are increased by 10%, 20% and 30% (parameter values are individually reduced to 110%, 120% and 130% of the nominal values as listed in Table 1). These results are presented in Fig. 10.

Similar to the cases where the system parameters were decreased (presented in Fig. 9), for the cases where system parameters are increased, the combined scheme still manages to maintain desired bit velocity. The trend in changes to the control input is also similar, albeit more pronounced. The desired bit velocity is still set to $\Omega_d = 3.5\ \mathrm{rad\,s^{-1}}$ and requires control inputs of 49.75 N m, 53.73 N m and 57.72 N m for system simulated with 110%, 120% and 130% of the nominal parameter values. What is also interesting to note is that when the system parameter values are less than nominal (Fig. 9), the control torque has a significant overshoot when compared to the cases where the system parameter values are greater. However, the transients settle down quicker compared to those manifesting when controlling a system with parameter values greater than the nominal (Fig. 10). To perform a comparative analysis of the proposed combined scheme, the recently proposed Sliding-Mode Controller (SMC) [54], that has emerged as a benchmark for control of drill-strings, is employed as a candidate. The next section introduces the SMC and tests the proposed combined scheme on a more complex drill-string.

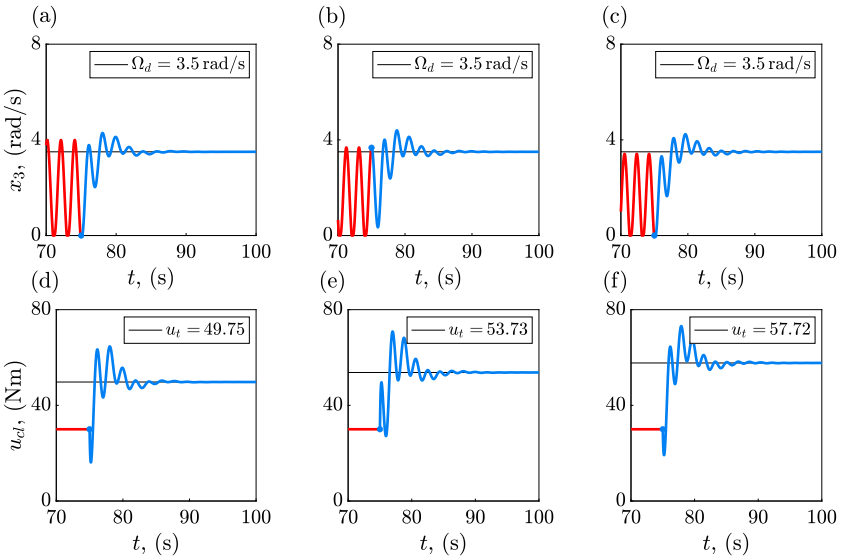

Fig. 10. Black solid lines represent target desired velocities and torques for respective plots. Time traces for bit velocity and corresponding control input for system with: (a and d) 110% of the nominal values. (b and e) 120% of the nominal values. (c and f) 130% of the nominal values.

6. Performance analysis of the proposed control scheme

In order to determine the performance of the proposed combined scheme, two subsections are introduced. Section 6.1. compares the proposed combined scheme directly to the previous state-of-the-art Sliding-Mode control and Section 6.2. evaluates the proposed combined scheme on an 8-DOF drill-string with much higher complexity and upscaled parameters.

6.1. Comparison with sliding-mode control

In this subsection, the SMC is defined and benchmarked against the proposed combined scheme. The SMC adopted as a candidate for comparison starts by defining a sliding surface given by [54]:

$$s = \left(x_1 - \Omega_d\right) + \Gamma \int_0^t \left(x_1 - \Omega_d\right) d\tau + \Gamma \int_0^t \left(x_1 - x_3\right) d\tau, \tag{28}$$

where Γ is a user chosen variable and Ω_d is the desired velocity. The key benefit of SMC is the capability of utilising estimated system parameters. The estimated parameters are denoted as; $\hat{c}_r$, $\hat{c}_s$, $\hat{k}_s$ and $\hat{J}_t$. The ideal controller equation can be derived by differentiating (28) and substituting it into Eq. (14) and rearranging for u. By replacing all original variables with their estimated ones, the estimated controlx input is shown to be:

$$u_{est} = \left(\hat{c}_r + \hat{c}_s\right) x_1 - \hat{c}_s x_3 + \hat{k}_s x_2 - \hat{J}_t \Gamma \left(x_1 - \Omega_d\right) - \hat{J}_t \Gamma \left(x_1 - x_3\right). \tag{29}$$

Additionally, the upper bounds of the estimated model are given as:

$$\|\hat{c}_r - c_r\| \le M_{cr}, \quad \|\hat{c}_s - c_s\| \le M_{cs}, \quad \|\hat{k}_s - k_s\| \le M_{ks}, \quad \|\hat{J}_t - J_t\| \le M_{jt}. \tag{30}$$

From this, the asymptotically convergent switching law is defined as:

$$\begin{aligned} u_{sw} = &- \frac{M_{cr}\|x_1 - x_3\| s}{\|s\| + \delta_1 \exp\left(-\delta_2 \int \|x_1 - x_3\| d\tau\right)} \\ &- \frac{M_{cs}\|x_1\| s}{\|s\| + \delta_1 \exp\left(-\delta_2 \int \|x_1\| d\tau\right)} + \cdots \\ &- \frac{M_{ks}\|x_2\| s}{\|s\| + \delta_1 \exp\left(-\delta_2 \int \|x_2\| d\tau\right)} \\ &- \frac{M_{jt}\Gamma\|x_1 - \Omega_d\| s}{\|s\| + \delta_1 \exp\left(-\delta_2 \int \Gamma\|x_1 - \Omega_d\| d\tau\right)} + \cdots \\ &- \frac{M_{jt}\Gamma\|x_1 - x_3\| s}{\|s\| + \delta_1 \exp\left(-\delta_2 \int \Gamma\|x_1 - x_3\| d\tau\right)} - \rho s, \end{aligned} \tag{31}$$

where $\delta_1 \ll 1$ and $\delta_2 \ll 1$ are small controller parameters and ρ is another user chosen control parameter. The final SMC control input is defined as:

$$u = u_{est} + u_{sw}. \tag{32}$$

A table (Table 4) for the SMC and proposed scheme parameters can be found in the Appendix. To compare the SMC to the proposed combined scheme, the cases shown in Fig. 8(c), (e) and (g) are simulated for both the SMC and combined scheme.

Three cases have been analysed in Fig. 11 as (i) Case 1 (a and e): System starts from an unstable stick–slip attractor at $u = 40$ N m and is driven to a stable constant drilling attractor occurring at a lower input level $u = 30$ N m. (ii) Case 2 (b and f): System starts from an unstable stick–slip attractor at $u = 40$ N m and is driven to a stable constant drilling attractor occurring at the same input level. (iii) Case 3 (c and g): System starts from an unstable stick–slip attractor at $u = 40$ N m and is driven to a stable constant drilling attractor occurring at a higher input value $u = 50$ N m. Both the SMC and combined scheme simulations begin with the same initial conditions for each simulation. The combined scheme and SMC are both switched on at $t = 75$ s. A cursory overview of the results shows that both controllers deliver almost equal performance. However, careful probing shows that for higher values of bit velocity, the transients in the bit velocity profiles (b and c) as well as the corresponding control input profiles (f and g) have a higher magnitude and manifest for longer time in case of the SMC. In this sense, the combined scheme is visibly superior. The combined scheme get more attractive when its simplicity of design is contrasted with that of the SMC. This simplicity arises from the fact that the combined scheme works independently of the system model and has a very simple structure comprising of four tunable gains and two first-order integral equations. On the other hand, SMC relies on complete knowledge of the system dynamics in order to produce acceptable results. Furthermore, the SMC is robust to system parameter uncertainties, but these uncertainties have to be directly embedded into the sliding surface and control input equations for this form of SMC; consequently increasing its complexity. In the following section, the combined scheme on an 8-DOF system is considered in order to prove its flexibility.

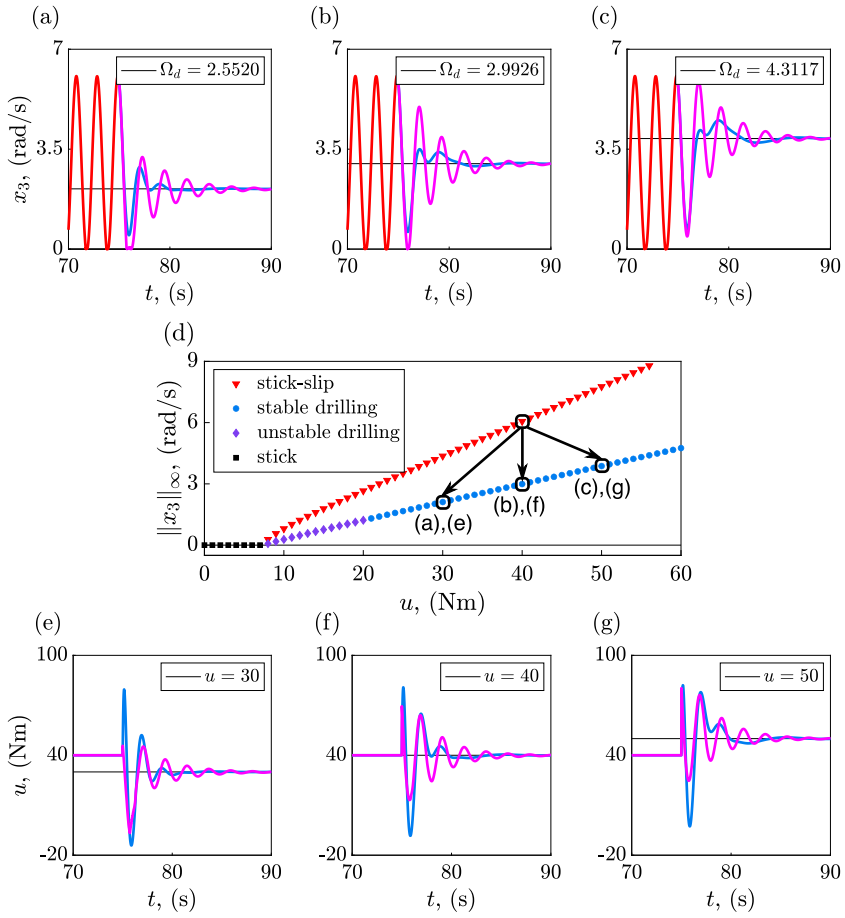

Fig. 11. Black solid lines represent target desired velocities and torques for respective plots. (a – c) Time traces of bit-velocity for the open-loop system as well as the closed-loop SMC controlled and combined scheme control systems when controllers are engaged at $t = 75$ s. (d) Bifurcation diagram of the overall open- and closed-loop system showing the stick, stick–slip and constant drilling phases. (e - g) Time traces for control inputs corresponding to the bit-velocity profiles presented in (a – c).

6.2. Efficacy of the proposed control scheme applied to an 8-DOF drill-string model

In this subsection an 8-DOF model, with large-scale parameters based on the model seen in [28], is used to verify the proposed scheme for suppression of stick–slip and tracking of a desired velocity in a more complicated system. This system used is an upscaled system compared to the previous one and utilises the same bit-rock model interaction as before. Its main inclusion is as a general proof of concept that the aforementioned control scheme works even on upscaled systems with much larger system parameters. It should be noted that the main 2-DOF system analysed in this work is not a subset of the following 8-DOF one. A table (Table 5) can be found with the upscaled parameters along with proposed scheme gains. The state-space that describe the 8-DOF closed-loop system dynamics are:

$$\dot{Z} = AZ + \frac{u}{J_t}B - \frac{T_b}{J_b}V + \Omega_d T, \tag{33}$$

where $Z, B, V, T \in \mathbb{R}^{15\times 1}$ and $A \in \mathbb{R}^{15\times 15}$. The expanded differential equations, Eqs (33), can be found in the Appendix.

As can be seen in Fig. 12, the combined scheme is capable of handling the higher complexity similar in the simpler 2-DOF case. This comes at the price of settling time due to the increase in system parameters as well as greatly increasing DOF order. This directly indicates its robustness to complexity thanks to its design topology not requiring precise system knowledge in order to function. The following section concludes the paper.

7. Closing remarks

In this work, a modified integral resonant controller with integral tracking is investigated on a 2-DOF drill-string. Firstly, the 2-DOF model with nonlinear bit-rock interaction is verified numerically in the form of a torque bifurcation diagrams. Time histories, combined with 2D and 3D phase portraits are shown in order to demonstrate the three main drilling responses available to the aforementioned model, namely: stick (no drilling), stick–slip (a limit cycle response) and constant drilling. Further to this, the bifurcation diagrams also reveal the co-existence of system solutions for a given torque and weight-on-bit, i.e. the co-existence of constant drilling and stick–slip. The ideal case of constant drilling is the desired response and is the main control focus in this work.

The scheme in question is subsequently introduced and it is able to successfully track to constant drilling when the drill-string is started in stick–slip. This is shown via a single test case demonstrating its positive damping effects with the time–history and 2-D/3-D phase-portraits results. The control input graph is also shown. A detailed investigation into the MIRC's ability to stabilise unstable constant drilling solutions is discussed in detail via the use of fundamental Hopf-Bifurcation theory. Then it is shown that the MIRC can be combined with integral tracking in order to track any desired drill-string velocity chosen. Subsequent to this, numerous cases from different starting points on the torque bifurcation diagram in to determine if the scheme runs into stick–slip on the way to any of the solutions. It is found that tracking is possible from almost any starting torque or initial condition even when tracking an unstable constant drilling solution. After this, a robustness analysis

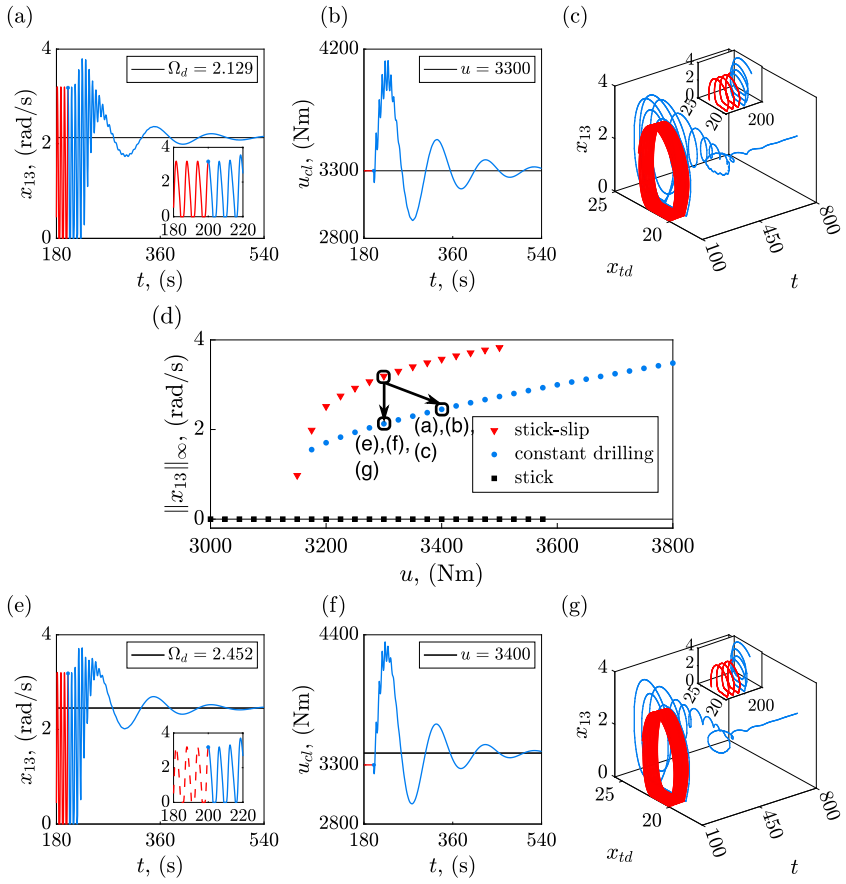

Fig. 12. Black solid lines represent target desired velocities and torques for respective plots. (d) Bifurcation diagram that shows the open-loop characteristics of the system and the regions of co-existing attractors. (a – c) and (e – g) Show time traces of bit-velocity for the closed-loop system, control input and 3-D phase-plane when the controller is engaged at $t = 200$ s for different desired velocities of $\Omega_d = 2.129$ rad s^{-1} and $\Omega_d = 2.452$ rad s^{-1} respectively. It is observed that the combined scheme is able to guide the 8-DOF system to its natural constant-drilling attractor or a higher target desired velocity.

is carried out on the combined scheme in order to see if it fails its task under the effects of increasing and decreasing system parameters. It is found to be successful in dealing with changing conditions.

The Sliding-Mode Controller is subsequently introduced as the previous state-of-the-art for comparing the scheme to. It is found that the SMC, when put under the same situations as proposed combined scheme, performs almost identically with the advantage that the proposed combined scheme is much simpler in its construction. This simplicity for the same performance is the greatest advantage over the SMC and its simplicity also allows for easy implementation of extra control schemes on the based MIRC scheme discussed. Furthermore, due to the complexity of real life drill-strings, an 8-DOF drill-string with upscaled parameters is simulated and put into closed-loop with the proposed combined scheme and successfully tracks two chosen desired velocities. The success found with a more complex and upscaled system is testament to the combined scheme's general design that does not require or rely on precise system models unlike the SMC.

Conclusively, the scheme has promising robustness to varying system parameters, itself to be superior to that of the previous state-of-the-art SMC due to delivering the same performance for less complexity while also not needing a detailed system model. Further work would include an experimental verification of the controller with extensive gain testing to confirm the simulations in this work.

CRediT authorship contribution statement

James D.J. MacLean: Conceptualization, Formulation and program for simulations, Writing – original draft. **Vahid Vaziri:** Conceptualization, Formulation and program for simulations, Writing – original draft. **Sumeet S. Aphale:** Conceptualization, Writing – original draft. **Marian Wiercigroch:** Conceptualization, Writing – original draft.

Declaration of competing interest

The authors declare that they have no known competing financial interests or personal relationships that could have appeared to influence the work reported in this paper.

Appendix A. Lagrangian MIRC Lyapunov stability

Consider the following closed-loop Lagrangian $\mathcal{L} : \mathbb{R}^{3\times1} \to \mathbb{R}$ which consists of the total kinetic energy $\mathcal{T}$ such that $\mathcal{L} : \mathbb{R}^{3\times1} \to \mathbb{R}$ and the total potential energy $\mathcal{U}$ such that $\mathcal{U} : \mathbb{R}^{3\times1} \to \mathbb{R}$ connected by the relation $\mathcal{L} = \mathcal{T} - \mathcal{U}$. In addition, there is also Rayleigh's Dissipation to consider $\mathcal{D} : \mathbb{R}^{3\times1} \to \mathbb{R}$. Consider the set of generalised coordinates $q_k = [\phi_t, \quad \phi_b, \quad \psi] \in \mathbb{R}^{3\times1}$ accompanied by a generalised forcing vector $\mathcal{G}_k$. Consider the total kinetic energy $\mathcal{T}$:

$$\mathcal{T} = \frac{1}{2}J_t\dot{\phi}_t^2 + \frac{1}{2}J_b\dot{\phi}_b^2 + \frac{1}{2}\int \dot{\psi}^2 dt, \tag{34}$$

the total potential energy $\mathcal{U}$:

$$\mathcal{U} = \frac{\kappa\eta}{2}\psi^2 + \frac{1}{2}k_s\left(\phi_t - \phi_b\right)^2, \tag{35}$$

Rayleigh's Dissipation Function $\mathcal{D}$:

$$\mathcal{D} = \frac{1}{2}c_r\dot{\phi}_t^2 + \frac{1}{2}c_s\left(\dot{\phi}_t - \dot{\phi}_b\right)^2, \tag{36}$$

and the generalised force vector $\mathcal{G}_k$ is then defined as:

$$\mathcal{G}_k = \left[u + \eta\psi, \quad -T_b, \quad -\lambda\left(\dot{\phi}_b - \dot{\phi}_t\right)\right]^T. \tag{37}$$

The Euler Lagrange Equation for this case of combining the scheme with the drill-string can be defined as follows:

$$\frac{\partial}{\partial t}\left(\frac{\partial \mathcal{L}}{\partial \dot{q}_k}\right) - \frac{\partial \mathcal{L}}{\partial q_k} + \frac{\partial \mathcal{D}}{\partial \dot{q}_k} = \mathcal{G}_k. \tag{38}$$

For each $k \in [1, 2, 3]$ and applying the Euler–Lagrange Equation for each case, the Eqs (10), (11) and (12) shown earlier.

Appendix B. MIRC Lyapunov analysis

To infer the scheme's stability, consider the following Lyapunov energy analysis. A Lyapunov candidate which enforces $V : \mathbb{R}^{4\times1} \to \mathbb{R}$ is subject to the following stability constraints, namely; $V(\bar{X}) = 0 : \bar{X} \in \mathbb{R}^{4\times1} = 0$, $V(\bar{X}) > 0 : \forall \bar{X} \in \mathbb{R}^{4\times1} \neq 0$ and $\dot{V}(\bar{X}) \leq 0 : \forall \bar{X} \in \mathbb{R}^{4\times1}$. A candidate which satisfies the first two constraints immediately is as follows:

$$V(\bar{X}) = \frac{1}{2}\left[J_t x_1^2 + k_s x_2^2 + J_b x_3^2 + x_4^2\right]. \tag{39}$$

To determine whether this candidate satisfies the third mentioned restriction, both equilibria of stick and constant drilling, are examined. By differentiating Eq. (39):

$$\dot{V}(\bar{X}) = J_t x_1 \dot{x}_1 + k_s x_2 \dot{x}_2 + J_b x_3 \dot{x}_3 + x_4 \dot{x}_4. \tag{40}$$

Substituting in the individual differential equations taken from the state-space Eq. (14) into (40):

$$\dot{V}(\bar{X}) = -\left[c_s + c_r\right] x_1^2 - c_s x_3^2 + 2c_s x_3 x_1 - \kappa\eta x_4^2 - \lambda\left[x_3 - x_1\right] x_4. \tag{41}$$

Now consider equilibria (17) and (18) substituted into Eq. (41) which results in the following:

$$\dot{V}(\bar{X}_{e,s}) = 0 \quad \text{and} \quad \dot{V}(\bar{X}_{e,c}) = -c_r \Omega_c^2 \tag{42}$$

Given that $c_r > 0$ and $\Omega_c > 0$ this implies that in the case of both equilibria that $\dot{V}(\bar{X}) \leq 0$, hence proving the third constraint mentioned and thereby proving stability. Moreover the system is locally asymptotically stable. It is locally asymptotically stable due to the fact that Eq. (41) is not radially unbounded. As $\|\bar{X}\| \to \infty$, the term $x_3 - x_1 \to 0$ which comes from the controller contribution. This implies radial boundedness and thereby local asymptotically stability in this case [61].

Appendix C. MIRC with integral tracking Lyapunov analysis

To infer the combined scheme's stability, consider the following Lyapunov energy analysis. A Lyapunov candidate which enforces $V : \mathbb{R}^{5\times1} \to \mathbb{R}$ is subject to the following stability constraints, namely; $V(\bar{X}) = 0 : \bar{X} \in \mathbb{R}^{5\times1} = 0$, $V(\bar{X}) > 0 : \forall \bar{X} \in \mathbb{R}^{5\times1} \neq 0$ and $\dot{V}(\bar{X}) \leq 0 : \forall \bar{X} \in \mathbb{R}^{5\times1}$. A candidate which satisfies the first two constraints immediately is as follows:

$$V(\bar{X}) = \frac{1}{2}\left[J_t x_1^2 + k_s x_2^2 + J_b x_3^2 + x_4^2 + x_5^2\right]. \tag{43}$$

To determine whether this candidate satisfies the third mentioned restriction, both equilibrium of constant drilling, is examined. By differentiating Eq. (43):

$$\dot{V}(\bar{X}) = J_t x_1 \dot{x}_1 + k_s x_2 \dot{x}_2 + J_b x_3 \dot{x}_3 + x_4 \dot{x}_4. \tag{44}$$

Substituting in the individual differential equations taken from the state-space Eq. (27) into (43):

$$\dot{V}(\bar{X}) = -\left[c_s + c_r\right] x_1^2 - c_s x_3^2 + 2c_s x_3 x_1 - \kappa\eta x_4^2 - \lambda\left[x_3 - x_1\right] x_4 - \left[x_1 - \Omega_d\right] x_5. \tag{45}$$

In order to determine whether the integral tracking loop affects the closed-loop stability, consider a desired constant-drilling velocity of Ω_d. To ensure tracking: $x_1 \to \Omega_d$ and $x_3 \to \Omega_d$. This modifies the constant drilling equilibria to:

$$\hat{X}_{c,trk} = \left[\Omega_d, \frac{u - c_r\Omega_d}{k_s}, \Omega_d, 0, \Lambda\right]^T, \tag{46}$$

Table 4
Values of SMC parameters.

Symbol	Name	Value
$\hat{c}_r$	Estimated top-drive damping coefficient	10.242
$\hat{c}_s$	Estimated torsional damping coefficient	0.0045
$\hat{k}_s$	Estimated torsional Stiffness coefficient	9
$\hat{J}_t$	Estimated top-drive inertia	12.573
M_{cr}	Upper bound of top-drive damping coefficient	1.393
M_{cs}	Upper bound of torsional damping coefficient	5×10^{-4}
M_{ks}	Upper bound of torsional stiffness coefficient	1
M_{jt}	Upper bound of top-drive inertia	1.138
Ω_d	Desired angular velocity	3.5
Γ	Integral gain	0.8
δ_1	Switching law constant one	1×10^{-2}
δ_2	Switching law constant two	1×10^{-5}
ρ	Switching law surface gain	1
λ	Output feedback gain	−10
η	Integrator gain	10
κ	Feed-through gain	1

where $\Lambda \in \mathbb{R}$. Now consider equilibria (46) and substitute it into Eq. (45):

$$\dot{V}(\bar{x}_{c,trk}) = -c_r \Omega_c^2. \tag{47}$$

Given that $c_r > 0$ and $\Omega_c > 0$, this follows that $\dot{V}(\bar{x}_{c,trk}) < 0$. Thus, the equilibrium for constant drilling is asymptotically stable. Hence, the inclusion of an integral tracking loop does not affect the closed-loop stability of the system. Moreover the system is locally asymptotically stable. It is locally asymptotically stable due to the fact that Eq. (45) is not radially unbounded. As $\|\bar{X}\| \to \infty$, the term $x_3 - x_1 \to 0$ which comes from the MIRC controller contribution of the combined scheme. This implies radial boundedness and thereby local asymptotically stability in this case [61].

Appendix D. SMC and proposed scheme parameters

See Table 4.

Appendix E

8-DOF system parameters

See Table 5.

Closed-loop 8-DOF equations

$$\dot{x}_1 = \frac{1}{J_t}\left[u + \eta x_{14} + k_i x_{15} - (c_p + c_{rt})x_1 + c_p x_3 - k_p x_2\right], \tag{48}$$

$$\dot{x}_2 = x_1 - x_3, \tag{49}$$

$$\dot{x}_3 = \frac{1}{J_n}\left[c_p x_1 - 2c_p x_3 + c_p x_5 + k_p x_2 - k_p x_4\right], \tag{50}$$

$$\dot{x}_4 = x_3 - x_5, \tag{51}$$

$$\dot{x}_5 = \frac{1}{J_n}\left[c_p x_3 - 2c_p x_5 + c_p x_7 + k_p x_4 - k_p x_6\right], \tag{52}$$

$$\dot{x}_6 = x_5 - x_7, \tag{53}$$

$$\dot{x}_7 = \frac{1}{J_n}\left[c_p x_5 - 2c_p x_7 + c_p x_9 + k_p x_6 - k_p x_8\right], \tag{54}$$

$$\dot{x}_8 = x_7 - x_9 \tag{55}$$

$$\dot{x}_9 = \frac{1}{J_n}\left[c_p x_7 - (c_p + c_r)x_9 + c_r x_{11} + k_p x_8 - k_r x_{10}\right], \tag{56}$$

$$\dot{x}_{10} = x_9 - x_{11}, \tag{57}$$

$$\dot{x}_{11} = \frac{1}{J_r}\left[c_p x_9 - (c_r + c_b)x_{11} + c_b x_{13} + k_r x_{10} - k_b x_{12}\right], \tag{58}$$

$$\dot{x}_{12} = x_{11} - x_{13}, \tag{59}$$

Table 5
8-DOF model parameters, values and units.

Symbol	Name	Value(s) and Units
μ_{cb}	Coulomb friction coefficient	0.45
μ_{sb}	Static friction coefficient	0.8
R_b	Bit radius	0.15 m
WOB	Weight-on-bit	30 000 N
γ_b	Velocity decrease rate	0.9
v_f	Velocity constant	1
ζ	Small positive constant	10^{-6}
u	Top-torque	$u = [3000, 3800]$ N m
J_t	Top-drive inertia	910 kg m^2
J_n	Pipe inertia	2800 kg m^2
J_r	Collar inertia	750 kg m^2
J_b	Bit inertia	450 kg m^2
c_{rt}	Top-drive damping coefficient	410 N m s rad^{-1}
c_n	Pipe damping coefficient	150 N m s rad^{-1}
c_r	Collar damping coefficient	190 N m s rad^{-1}
c_b	Bit damping coefficient	180 N m s rad^{-1}
c_{rb}	Bit-wall damping coefficient	80 N m s rad^{-1}
k_n	Pipe stiffness coefficient	700 N m rad^{-1}
k_r	Collar stiffness coefficient	1080 N m rad^{-1}
k_b	Bit stiffness coefficient	910 N m rad^{-1}
λ	Output feedback gain	50
η	Integrator gain	10
κ	Feed-through gain	1.5
k_i	Tracking gain	50

$$\dot{x}_{13} = \frac{1}{J_b}\left[c_b x_{11} - (c_b + c_{rb})x_{13} + k_b x_{12} - T_b\right], \tag{60}$$

$$\dot{x}_{14} = -\kappa\eta x_{14} - \lambda\left[x_{13} - x_1\right], \tag{61}$$

$$\dot{x}_{15} = \Omega_d - x_{13}. \tag{62}$$

References

[1] Chin WC. Advanced system summary and modern MWD developments. In: Measurement while drilling (MWD) signal analysis, optimization, and design. 2018, http://dx.doi.org/10.1002/9781119479307.ch10.

[2] Kapitaniak M, Hamaneh VV, Wiercigroch M. Torsional vibrations of helically buckled drill-strings: Experiments and FE modelling. J Phys Conf Ser 2016;721(1). http://dx.doi.org/10.1088/1742-6596/721/1/012012.

[3] Khulief YA, Al-Naser H. Finite element dynamic analysis of drillstrings. Finite Elem Anal Des 2005. http://dx.doi.org/10.1016/j.finel.2005.02.003.

[4] Jansen JD, van den Steen L. Active damping of self-excited torsional vibrations in oil well drillstrings. J Sound Vib 1995. http://dx.doi.org/10.1006/jsvi.1995.0042.

[5] Hajianmaleki M, Daily JS, Ring L, Gandikota R. Critical buckling load assessment of drill strings in different wellbores using the explicit finite element method. In: Society of petroleum engineers - SPE offshore europe conference and exhibition, OE 2013. 2013, http://dx.doi.org/10.2118/166592-ms.

[6] Sangeetha N, Sathish Kumar P. A study of vibration analysis for drill string using finite element analysis. IOSR J Mech Civ Eng 2014.

[7] Kapitaniak M, Vaziri V, Páez Chávez J, Wiercigroch M. Experimental studies of forward and backward whirls of drill-string. Mech Syst Signal Process 2018;100:454–65. http://dx.doi.org/10.1016/j.ymssp.2017.07.014, URL: http://www.sciencedirect.com/science/article/pii/S0888327017303746.

[8] Hohl A, Tergeist M, Oueslati H, Herbig C, Ichaoui M, Ostermeyer GP, Reckmann H. Prediction and mitigation of torsional vibrations in drilling systems. In: SPE/IADC drilling conference, proceedings. 2016, http://dx.doi.org/10.2118/178874-ms.

[9] Jardine S, Malone D, Sheppard M. Putting a damper on drilling's bad vibrations. Oilfield Rev 1994.

[10] Christoforou AP, Yigit AS. Fully coupled vibrations of actively controlled drillstrings. J Sound Vib 2003. http://dx.doi.org/10.1016/S0022-460X(03)00359-6.

[11] Liu W, Zhou Y, Zhao Q. A new analytical model on lateral vibration and impact of drill string, In: Proceedings of the International Offshore and Polar Engineering Conference, 2010.

[12] Xue Q, Wang R, Sun F. 1367. Study On lateral vibration of rotary steerable drilling system. J Vibroeng 2014;16(6):2702–11.

[13] Perng YL, Chin JH. Theoretical and experimental investigations on the spinning bta deep-hole drill shafts containing fluids and subject to axial forces. Int J Mech Sci 1999. http://dx.doi.org/10.1016/S0020-7403(98)00091-5.

[14] Khulief YA, Al-Sulaiman FA, Bashmal S. Vibration analysis of drillstrings with self-excited stick-slip oscillations. J Sound Vib 2007. http://dx.doi.org/10.1016/j.jsv.2006.06.065.

[15] Ahmadi K, Altintas Y. Stability of lateral, torsional and axial vibrations in drilling. Int J Mach Tools Manuf 2013;68:63–74. http://dx.doi.org/10.1016/j.ijmachtools.2013.01.006.

[16] Beck FE, Boone DE, DesBrandes R, Wojtanowicz AK, Johnson PW, Lyons WC, Miska S, Mujeeb A, Nathan C, Russell CS, Shahraki AK. Drilling and well completions. In: Standard handbook of petroleum and natural gas engineering. 1996, http://dx.doi.org/10.1016/b978-088415642-0.50005-9.

[17] Haldar S. Chapter 7 – sampling methods. Mineral Explor 2013;117–35. http://dx.doi.org/10.1016/B978-0-12-416005-7.00007-6.

[18] Ma T, Chen P, Zhao J. Overview on vertical and directional drilling technologies for the exploration and exploitation of deep petroleum resources. 2016, http://dx.doi.org/10.1007/s40948-016-0038-y.

[19] Wang H, Ge Y, Shi L. Technologies in deep and ultra-deep well drilling: Present status, challenges and future trend in the 13th five-year plan period (2016–2020). Nat Gas Ind B 2017;4(5):319–26. http://dx.doi.org/10.1016/j.ngib.2017.09.001.

[20] Zhang Z-X. Rock drilling and boring. Rock Fracture Blasting 2016;155–75. http://dx.doi.org/10.1016/b978-0-12-802688-5.00007-5.

[21] Spanos PD, Chevallier AM, Politis NP, Payne ML. Oil and gas well drilling: A vibrations perspective. 2003, http://dx.doi.org/10.1177/0583102403035002564.

[22] Zhu X, Liu W. The effects of drill string impacts on wellbore stability. J Pet Sci Eng 2013. http://dx.doi.org/10.1016/j.petrol.2013.08.004.

[23] Ledgerwood LW, Hoffmann OJ, Jain JR, El Hakam C, Herbig C, Spencer RW. Downhole vibration measurement, monitoring and modeling reveal stick-slip as a primary cause of PDC bit damage in today's applications, In: Proceedings - SPE Annual Technical Conference and Exhibition, 2010.

[24] Liao CM, Vlajic N, Karki H, Balachandran B. Parametric studies on drill-string motions. Int J Mech Sci 2012. http://dx.doi.org/10.1016/j.ijmecsci.2011.11.005.

[25] Schwefe T, Ledgerwood LW, Jain JR, Fuselier DM, Oueslati H, Endres L. Development and testing of stick/slip-resistant PDC bits. In: SPE/IADC drilling conference, proceedings. 2014, http://dx.doi.org/10.2118/168026-ms.

[26] Navarro-López EM, Cortés D. Avoiding harmful oscillations in a drillstring through dynamical analysis. J Sound Vib 2007. http://dx.doi.org/10.1016/j.jsv.2007.06.037.

[27] Navarro-López EM. An alternative characterization of bit-sticking phenomena in a multi-degree-of-freedom controlled drillstring. Nonlinear Anal RWA 2009. http://dx.doi.org/10.1016/j.nonrwa.2008.10.025.

[28] Navarro-López EM, Licéaga-Castro E. Non-desired transitions and sliding-mode control of a multi-dof mechanical system with stick-slip oscillations. Chaos Solitons Fractals 2009. http://dx.doi.org/10.1016/j.chaos.2008.08.008.

[29] Liu X, Vlajic N, Long X, Meng G, Balachandran B. Nonlinear motions of a flexible rotor with a drill bit: Stick-slip and delay effects. Nonlinear Dynam 2013. http://dx.doi.org/10.1007/s11071-012-0690-x.

[30] Liu X, Long X, Zheng X, Meng G, Balachandran B. Spatial-temporal dynamics of a drill string with complex time-delay effects: Bit bounce and stick-slip oscillations. Int J Mech Sci 2020;170:105338. http://dx.doi.org/10.1016/j.ijmecsci.2019.105338, URL: https://www.sciencedirect.com/science/article/pii/S0020740319327560.

[31] Fu M, Zhang P, Li J, Wu Y. Observer and reference governor based control strategy to suppress stick-slip vibrations in oil well drill-string. J Sound Vib 2019;457:37–50. http://dx.doi.org/10.1016/j.jsv.2019.05.050, URL: http://www.sciencedirect.com/science/article/pii/S0022460X19303190.

[32] Zheng X, Agarwal V, Liu X, Balachandran B. Nonlinear instabilities and control of drill-string stick-slip vibrations with consideration of state-dependent delay. J Sound Vib 2020;473:115235. http://dx.doi.org/10.1016/j.jsv.2020.115235, URL: http://www.sciencedirect.com/science/article/pii/S0022460X20300663.

[33] Wiercigroch M, Nandakumar K, Pei L, Kapitaniak M, Vaziri V. State dependent delayed drill-string vibration: Theory, experiments and new model. Proc IUTAM 2017;22:39–50. http://dx.doi.org/10.1016/j.piutam.2017.08.007, URL: http://www.sciencedirect.com/science/article/pii/S2210983817300962.

[34] Selnes KS, Clemmensen C, Reimers N. Drilling difficult formations efficiently with the use of an antistall tool. In: SPE/IADC drilling conference, proceedings. 2008, http://dx.doi.org/10.2118/111874-ms.

[35] Seines KS, Clemmensen C, Reimers N. Drilling difficult formations efficiently with the use of an antistall tool. SPE Drilling and Completion 2009. http://dx.doi.org/10.2118/111874-pa.

[36] Vromen T, Detournay E, Nijmeijer H, Van De Wouw N. Dynamics of drilling systems with an antistall tool: Effect on rate of penetration and mechanical specific energy. SPE J 2019. http://dx.doi.org/10.2118/194487-PA.

[37] Karkoub M, Zribi M, Elchaar L, Lamont L. Robust μ-synthesis controllers for suppressing stick-slip induced vibrations in oil well drill strings. Multibody Syst Dyn 2010. http://dx.doi.org/10.1007/s11044-009-9179-x.

[38] Vromen T, Dai CH, Van De Wouw N, Oomen T, Astrid P, Nijmeijer H. Robust output-feedback control to eliminate stick-slip oscillations in drill-string systems. In: IFAC-PapersOnLine. 2015, http://dx.doi.org/10.1016/j.ifacol.2015.08.042.

[39] Vromen T, Dai CH, Van De Wouw N, Oomen T, Astrid P, Doris A, Nijmeijer H. Mitigation of torsional vibrations in drilling systems: A robust control approach. IEEE Trans Control Syst Technol 2019. http://dx.doi.org/10.1109/TCST.2017.2762645.

[40] Canudas-de Wit C, Rubio FR, Corchero MA. D-OSKIL: A new mechanism for controlling stick-slip oscillations in oil well drillstrings. IEEE Trans Control Syst Technol 2008. http://dx.doi.org/10.1109/TCST.2008.917873.

[41] Al Sairafi FA, Al Ajmi KE, Yigit AS, Christoforou AP. Modeling and control of stick slip and bit bounce in oil well drill strings. In: Proceedings of the SPE/IADC middle east drilling technology conference and exhibition. 2016, http://dx.doi.org/10.2118/178160-ms.

[42] Mfoumou GS, Kenmoé GD, Kofané TC. Computational algorithms of time series for stick-slip dynamics and time-delayed feedback control of chaos for a class of discontinuous friction systems. Mech Syst Signal Process 2019. http://dx.doi.org/10.1016/j.ymssp.2018.09.034.

[43] Wasilewski M, Pisarski D, Konowrocki R, Bajer CI. A new efficient adaptive control of torsional vibrations induced by switched nonlinear disturbances. Int J Appl Math Comput Sci 2019. http://dx.doi.org/10.2478/amcs-2019-0021.

[44] Hong L, Girsang IP, Dhupia JS. Identification and control of stick-slip vibrations using Kalman estimator in oil-well drill strings. J Pet Sci Eng 2016. http://dx.doi.org/10.1016/j.petrol.2016.01.017.

[45] Kamel MA, Elkatatny S, FaizanMysorewala M, Al-Majed A, Elshafei M. Adaptive and real-time optimal control of stick-slip and bit wear in autonomous rotary steerable drilling. J Energy Resour Technol Trans ASME 2018. http://dx.doi.org/10.1115/1.4038131.

[46] Zheng X, Agarwal V, Liu X, Balachandran B. Nonlinear instabilities and control of drill-string stick-slip vibrations with consideration of state-dependent delay. J Sound Vib 2020. http://dx.doi.org/10.1016/j.jsv.2020.115235.

[47] Bisoffi A, Beerens R, Heemels W, Nijmeijer H, van de Wouw N, Zaccarian L. To stick or to slip: A reset PID control perspective on positioning systems with friction. Annu Rev Control 2020. http://dx.doi.org/10.1016/j.arcontrol.2020.04.010, URL: http://www.sciencedirect.com/science/article/pii/S1367578820300201.

[48] Ritto TG, Ghandchi-Tehrani M. Active control of stick-slip torsional vibrations in drill-strings. JVC/J Vib Control 2019. http://dx.doi.org/10.1177/1077546318774240.

[49] Navarro-López EM, Suárez R. Practical approach to modelling and controlling stick-slip oscillations in oilwell drillstrings. In: Proceedings of the IEEE international conference on control applications. 2004, http://dx.doi.org/10.1109/cca.2004.1387580.

[50] Pavone DR, Desplans JP. Application of high sampling rate downhole measurements for analysis and cure of stick-slip in drilling. In: Proceedings - SPE annual technical conference and exhibition. 1994, http://dx.doi.org/10.2523/28324-ms.

[51] Monteiro HL, Trindade MA. Performance analysis of proportional-integral feedback control for the reduction of stick-slip-induced torsional vibrations in oil well drillstrings. J Sound Vib 2017. http://dx.doi.org/10.1016/j.jsv.2017.03.013.

[52] Tian J, Zhou Y, Yang L, Hu S. Analysis of stick-slip reduction for a new torsional vibration tool based on PID control. Proc Inst Mech Eng Part K 2020. http://dx.doi.org/10.1177/1464419319876397.

[53] Hernandez-Suarez R, Puebla H, Aguilar-Lopez R, Hernandez-Martinez E. An integral high-order sliding mode control approach for stick-slip suppression in oil drillstrings. Pet Sci Technol 2009. http://dx.doi.org/10.1080/10916460802455483.

[54] Vaziri V, Kapitaniak M, Wiercigroch M. Suppression of drill-string stick-slip vibration by sliding mode control: Numerical and experimental studies. European J Appl Math 2018. http://dx.doi.org/10.1017/S0956792518000232.

[55] MacLean JD, Aphale SS. A modified linear integral resonant controller for suppressing jump-phenomenon and hysteresis in micro-cantilever beam structures. J Sound Vib 2020;480:115365. http://dx.doi.org/10.1016/j.jsv.2020.115365, URL: http://www.sciencedirect.com/science/article/pii/S0022460X20301966.

[56] Namavar M, Fleming AJ, Aleyaasin M, Nakkeeran K, Aphale SS. An analytical approach to integral resonant control of second-order systems. IEEE/ASME Trans Mechatronics 2014. http://dx.doi.org/10.1109/TMECH.2013.2253115.

[57] Omidi E, Mahmoodi SN. Nonlinear vibration suppression of flexible structures using nonlinear modified positive position feedback approach. Nonlinear Dynam 2014. http://dx.doi.org/10.1007/s11071-014-1706-5.

[58] Li H, Liu S, Chang H. Experimental research on the influence of working parameters on the drilling efficiency. Tunnell Undergr Space Technol 2020;95:103174. http://dx.doi.org/10.1016/j.tust.2019.103174, URL: http://www.sciencedirect.com/science/article/pii/S0886779818307478.

[59] Shangxin F, Yujie W, Guolai Z, Yufei Z, Shanyong W, Ruilang C, Enshang X. Estimation of optimal drilling efficiency and rock strength by using controllable drilling parameters in rotary non-percussive drilling. J Pet Sci Eng 2020;193:107376. http://dx.doi.org/10.1016/j.petrol.2020.107376, URL: http://www.sciencedirect.com/science/article/pii/S0920410520304496.

[60] Pereira E, Aphale SS, Feliu V, Moheimani SO. Integral resonant control for vibration damping and precise tip-positioning of a single-link flexible manipulator. IEEE/ASME Trans Mechatronics 2011. http://dx.doi.org/10.1109/TMECH.2009.2039713.

[61] Murray RM, Li Z, Sastry SS. A mathematical introduction to robotic manipulation. 1994.